Towards a Novel Physics-Based Correction to Amiet's Theory for Inflow-Turbulence Noise Prediction

Towards a Novel Physics-based Correction to Amiet's Theory for Inflow-turbulence Noise Prediction

Andrea Piccolo*
Delft University of Technology, Delft, 2629HS, Netherlands

Riccardo Zamponi†
Delft University of Technology, Delft, 2629HS, Netherlands
von Kármán Institute for Fluid Dynamics, Sint-Genesius-Rode, B-1640, Belgium

Francesco Avallone‡
Politecnico di Torino, Torino, 10129, Italy

Daniele Ragni§
Delft University of Technology, Delft, 2629HS, Netherlands

A physical analysis has been conducted to assess the effects of turbulence distortion on leading-edge noise generation and low-fidelity modeling in the framework of Amiet's theory. This model retrieves the power spectral density (PSD) of far-field noise using as input the upwash velocity spectrum of incoming turbulent flow and an aeroacoustic transfer function modeling the aerodynamic and acoustic response of the airfoil to the perturbation. The study has been carried out by investigating the interaction of grid-generated turbulence with a NACA 0012 and a NACA 0012-103, featuring the same thickness but different leading-edge shape. The alteration of the velocity field has been shown to occur in agreement with the analytical findings of the rapid distortion theory (RDT), identifying in particular an exponential decay for the upwash-velocity component spectrum at high frequencies. The same decay is observed for the surface-pressure spectra close to the leading edge, suggesting that sound is generated by a pressure distribution induced by the altered velocity field and hence proving that turbulence-distortion effects should be included to enhance the noise-prediction accuracy of low-fidelity models. This has been further demonstrated by using as input in Amiet's model the altered upwash velocity spectrum sampled in the immediate vicinity of the leading edge: an improved prediction of the high-frequency decay is yielded, but the evident overestimation of the noise levels with respect to the results provided by the Ffowcs-Williams and Hawkings' (FWH) analogy indicates the necessity of correcting the aeroacoustic transfer function as well.

I. Introduction

The theory formulated by Amiet [1] provides a low-fidelity prediction of inflow-turbulence noise, or leading-edge noise, generated by the interaction of incoming turbulent structures with the front part of the airfoil.

This analytical relation, widely employed and investigated because of its accuracy and low computational cost, models the perturbation as a sinusoidal gust, with the far-field noise obtained using a transfer function characterizing the acoustic response of the airfoil, modeled as a flat plate. In the assumption of large airfoil span, the PSD of the far-field acoustic pressure S_{pp} at a listener position $\boldsymbol{x} = (x, y, z)$ is obtained through the following expression

$$\underbrace{S_{pp}\left(x, y, 0, \omega\right)}_{\text{PSD far-field noise}} = \underbrace{\left(\frac{\omega y \rho_\infty c}{2 c_\infty \sigma_0^2}\right)^2 \pi U_\infty \frac{L}{2}}_{\text{Flow and geometry characteristics}} \cdot \underbrace{\left|\mathcal{L}\left(\boldsymbol{x}, K_x, 0\right)\right|^2}_{\text{Aeroacoustic transfer function}} \cdot \underbrace{\Theta_{vv}\left(\omega\right) l_z\left(\omega\right)}_{\text{Turbulence characteristics}}, \tag{1}$$

*PhD Candidate, Flow Physics and Technology Department, a.piccolo@tudelft.nl.

†Assistant Professor, Flow Physics and Technology Department, r.zamponi@tudelft.nl, AIAA Member.

‡Full Professor, Department of Mechanical and Aerospace Engineering, francesco.avallone@polito.it, AIAA Member.

§Associate Professor, Flow Physics and Technology Department, d.ragni@tudelft.nl, AIAA Member.

where $K_x = -\omega/U_\infty$ is the streamwise wavenumber in the assumption of frozen turbulence, c and L are respectively the chord and the span of the airfoil, ρ_∞ is the density of the flow, the free-stream velocity is U_∞, and c_∞ is the speed of sound. As shown in the equation, the far-field noise prediction is related to the turbulence conditions, modeled through the frequency spectrum and the spanwise coherence length of the upwash velocity component, through the aeroacoustic transfer function $\mathcal{L}$. Further details about Amiet's theory and its derivation are reported in Appendix B.

The noise prediction obtained was shown to be in satisfactory agreement with the experimental measurements in the case of thin airfoils, becoming unreliable as the thickness increases or as the flow speed decreases, especially in the high-frequency range [2–4]. This was attributed to the fact that effects due to realistic airfoil geometry [2, 3, 5–8] and the consequent impact on the flow field [7, 9] were not properly characterized.

The distortion of the turbulence structures caused by the presence of a solid surface, in particular, has been largely investigated to define and model its possible impact on leading-edge noise generation. Most of these studies were based on the findings of the rapid distortion theory (RDT) formulated by Hunt [10], who analytically modeled the deformation undergone by turbulent eddies of size L_x in the interaction with a cylinder with characteristic dimension a. The extension of these results to realistic airfoil geometries and aeroacoustic applications has been made possible thanks to the work of Mish and Devenport [11, 12], who found that, by focusing on the flow field in the vicinity of the stagnation point, the airfoil can be considered as a cylinder with the same radius as the leading-edge circle.

Moreau and Roger [13] have been the first to try to implement the findings of the RDT for the enhancement of Amiet's model. The authors proposed a modification of the von Kármán spectrum decay slope in the high-frequency range from $-5/3$ to $-10/3$, in order to better model the distortion behavior of small-scale turbulent structures. Despite the validity of the correction was limited to the case in analysis, as specified by the same authors, this approach provided good agreement with the experimental measurements, paving the way for further developments of this methodology. In particular, Christophe [14], De Santana et *al.* [15] and Dos Santos et *al.* [16, 17] formulated correction factors for von Kármán spectrum which led to promising results when compared with experimental data. However, they also highlighted how the reliability of their procedure was limited by the necessity of identifying a representative position in the flow field to calculate turbulence characteristics, such as integral length scale and turbulence intensity.

Piccolo et *al.* [18] followed a different approach by implementing Amiet's model using as input a turbulence spectrum directly sampled in the stagnation region, where turbulence distortion occurs. In a rod-airfoil configuration, characterized by large-scale turbulence interacting with a NACA 0012, the spectrum was sampled at the position along the airfoil surface where the root-mean-square of the pressure fluctuation is maximum, yielding a good agreement with the prediction provided by the Ffwocs-Williams and Hawkings (FWH) analogy.

The purpose of the present work is to assess the effects induced by turbulence distortion that must be kept into account for low-fidelity noise prediction of leading-edge noise. The goal is to provide a comprehensive framework to enhance the accuracy of Amiet's model in the case of thick airfoil geometries.

This investigation has been carried out by analyzing numerically the interaction of grid-generated turbulence with a NACA 0012 and a NACA 0012-103, featuring a larger leading-edge radius, in order to assess the effect of airfoil geometry on turbulence distortion and noise generation. The study has been conducted employing the Lattice-Boltzmann Method (LBM) solver PowerFLOW. The numerical domain reproduces the experimental set-up utilized by Chaitanya at the University of Southampton for leading-edge noise analysis [8].

The layout of the paper is the following: Section II introduces the LBM solver PowerFLOW and details the computational domain, while the results of this physical investigation are reported in Section III. The conclusions are summarized in Section IV, and two appendices provide further information about the grid-independence study of the simulations (Appendix A) and Amiet's theory (Appendix B).

II. Methodology

A. Flow solver

The Lattice-Boltzmann Method (LBM) solver Simulia PowerFLOW 6-2021 has been used to run the numerical simulations of the two airfoils. The flow field is obtained by calculating the advection and the collision of fluid particles employing a statistical gas kinetic model, which, under the hypotheses of perfect gas at low Mach numbers and isothermal conditions, was proven to be an accurate methodology for the approximation of the Navier-Stokes equation [19]. The advection and the collision of the fluid particles, considered to occur along a finite number of predefined directions, are described by particle-distribution functions, from which the flow quantities are retrieved through local integration [20]. The software discretizes the Boltzmann equation on a Cartesian mesh, defined as *lattice*, by using

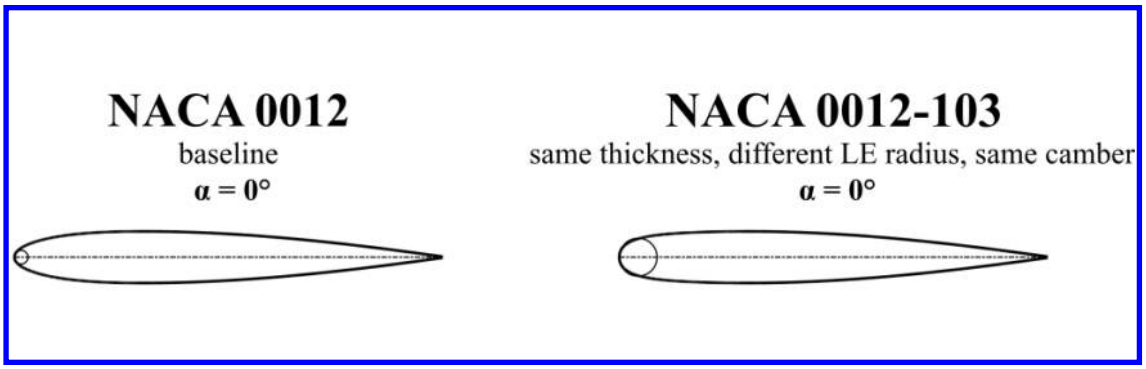

Fig. 1 The present work compares the interaction of incoming turbulence with a standard NACA 0012 and a NACA 0012-103, featuring the same thickness but a different leading-edge radius.

19 discrete velocity vectors in three dimensions, i.e. D3Q19, with a third-order truncation of the Chapman-Enskog expansion. The Bhatnagar-Gross-Krook (BGK) model [21], calculated as a function of the relaxation time, has been used to develop the collision operator.

PowerFLOW uses a very-large-eddy turbulence model to compute sub-grid unresolved turbulence scales. The calculation employs a modified $k-\epsilon$ two-equation re-normalization group formulation to derive an effective relaxation time, denoted as τ_{eff}. This effective relaxation time is obtained by combining the turbulent relaxation time with the viscous one [22]. This adjustment serves the purpose of preventing numerical damping of large-scale structures through the subgrid-scale viscosity mitigation [23]. Large-scale eddies develop by "updating" the Boltzmann model to the characteristic time scales of the turbulence in the flow through this modified relaxation time τ_{eff}.

The three-dimensional lattice is composed of unit elements defined voxels (volumetric pixel), while the surface elements obtained from the intersection of this grid with solid walls are referred to as surfels (surface elements). A wall function is applied by the software to increase the computational efficiency of the solver.

Far-field noise calculation is provided by means of Ffowcs-Williams and Hawkings' (FWH) acoustic analogy, implemented in the formulation 1A of Farassat and Succi [24] with forward-time solution [25]. In the current investigation, far-field noise has been obtained by sampling pressure fluctuations directly on the airfoil surface, meaning that the contribution of acoustic dipoles and monopoles distributions [26] to the noise generation has been taken into account while the one from non-linear contributions, i.e. quadrupole sources, has been neglected.

B. Simulation set-up

The simulation domain has been designed to reproduce the open-jet facility at the Institute of Sound and Vibration Research (ISVR) at the University of Southampton, where the reference experimental campaign of Chaitanya et al. [8] has been carried out.

Among the different airfoil geometries investigated by Chaitanya et al. [8], a NACA 0012 and a NACA 0012-103, characterized by the same thickness but a different length for the leading-edge radius (equal in this case to 2.4×10^{-3} m for the NACA 0012 and to 6.6×10^{-3} m for the NACA 0012-103), have been selected to carry out the investigation. The different leading-edge shape allows the analysis of the impact of this geometrical feature on the distortion of the incoming turbulent structures, conducted to determine the effects of this mechanism on leading-edge noise generation. The airfoils are shown in fig. 1.

The simulation domain is a cube with a side of 5 m, whose origin is coincident with the position of the leading edge of the airfoil. This has a rectangular planform with a chord c = 0.15 m and a span of L = 0.45 m and is placed at a zero angle of attack. The open-jet wind tunnel consists of a rectangular convergent nozzle of length 1.35 m, prolonged in the rear part with a rectangular duct in order to assign the boundary conditions on the external wall of the numerical domain. The inlet section is a square of side 1.3 m, while the exit section is a rectangle 0.45 m wide and 0.15 m high. With respect to the airfoil, the exit section is placed 1 chord upstream. Two rectangular plates 0.225 m long and 0.375 m high are positioned at the nozzle exit, on the two sides of the airfoil, to prevent aerodynamic tip effects. A qualitative representation of the numerical set-up is shown in fig. 2.

The free-stream velocity at the exit of the open-jet wind tunnel is equal to 59.5 m s^{-1}, measured at $x/c = -0.033$ upstream of the origin of the numerical domain in the simulation without the airfoil. This value is satisfactorily close

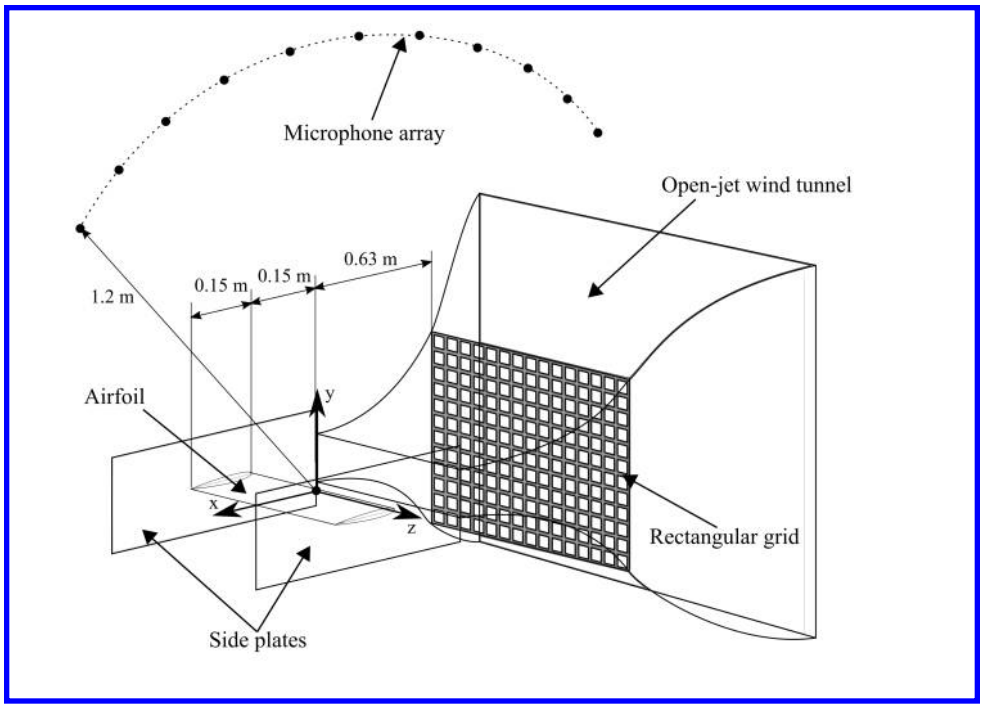

Fig. 2 Representation of the set-up of the two simulations. The relative dimensions are not drawn to scale.

Table 1 Turbulence characteristics at $x/c = -0.033$ in the configuration without the airfoil. The data obtained in the numerical simulation are compared with the measurements of the experimental campaign of Chaitanya et al. [8].

	$\overline{U}_\infty$	Tu_u	L^x_{uu}
	$(m\,s^{-1})$	(%)	(m)
Present study (PowerFLOW, LBM solver)	59.5	2.2	6.0×10^{-3}
Chaitanya et al. [8] (Exp.)	60	2.5	7.5×10^{-3}

to the one obtained in the reference experimental campaign, where the free-stream velocity is equal to $60\,m\,s^{-1}$. The Reynolds number with respect to the chord corresponding to the velocity obtained at the exit of the nozzle is equal to $Re = 6.2 \times 10^5$. This flow condition has been obtained by neglecting the friction loss along the walls of the nozzle and by setting the total pressure at the nozzle inlet, while the static pressure has been set to 101 325 Pa on the other boundaries of the domain.

Turbulence is generated by means of a rectangular grid 0.46 m high and 0.61 m wide, positioned in the final part of the open-jet wind tunnel 0.63 m upstream of the exit section. The rods, separated by a distance equal to 0.034 m, have a square section with a thickness of 0.012 m. This results in a solidity equal to 55 %. The pressure loss through the turbulence-generating grid has been accounted for through the empirical relations from Roach [27] to set the total pressure at the nozzle inlet.

In the numerical simulations, the rectangular grid yields an integral length scale L^x_{uu} of the incoming turbulence equal to 0.006 m, while the turbulence intensity of the streamwise velocity component is equal to 2.2 %. The reference values in the experimental campaign of Chaitanya et al. [8] are equal to 0.0075 m and 2.5 %, respectively, proving a good agreement between the simulations and the experimental data. The comparison between the flow characteristics obtained numerically and experimentally is reported in 1.

The numerical domain is discretized using different voxel-refinement regions, whose number depends on the resolution set for the simulation. In the finest configuration, 10 voxel-refinement regions are employed, which corresponds to an overall number of voxels 660×10^6. The turbulence-generating grid and the airfoil are placed in the same refinement region to prevent numerical effects from affecting the convection of turbulence structures. The

Table 2 Sampling locations of the velocity components along the stagnation streamline.

x [m]	x/c [−]
−0.75	−0.50
-7.50×10^{-3}	−0.050
-2.25×10^{-3}	−0.015
-1.50×10^{-5}	-1.00×10^{-4}

resolution is further decreased at the airfoil surface by adding two refinement regions obtained as offset of the surface itself. The smallest voxel size is hence equal to 1.79×10^{-4} m, which corresponds to a y^+ spatially averaged along the body of 19.

The duration of the simulation has been set in order to repeat 10 times the cycle at the lowest frequency taken into account (60 Hz). This results in an overall duration of 0.167 s with a physical time-step of 3.046×10^{-7} s. The flow field has been saved after waiting for a transient of 0.0625 s, whose duration has been defined by checking the convergence of the total pressure at the inlet of the open-jet wind tunnel.

The solid formulation of the FWH acoustic analogy has been employed to calculate far-field acoustic pressure. The analogy has been implemented by considering the pressure fluctuations on the airfoil surface, as explained in section II.A. The unsteady pressure distribution has been sampled at 30 kHz, as all the other flow quantities in the flow field. Far-field noise has been also measured directly by means of 11 direct probes. Considering a polar reference system centered at the airfoil leading edge with the azimuthal angle θ referred to the downstream direction, these probes are placed at a distance R = 1.2 m between $\theta = 40°$ and $\theta = 140°$.

As regards the calculation of the PSDs, these have been obtained by means of the Welch's method employing a Hanning window with a 50 % overlap. A 100 Hz frequency resolution has been set for the spectra.

The grid-independence study has been reported in detail in Appendix A.

III. Results

A. Alteration of the upwash-velocity spectrum and impact on the surface pressure

Frequency spectra of the streamwise and upwash velocity components are analyzed at different distances from the leading edge to assess possible alterations due to the turbulence distortion in the interaction with the airfoil. The sampling positions are reported in table 2. The analytical expressions formulated by von Kármán for the streamwise velocity component

$$\Theta_{uu}(k_x) = \frac{1}{\sqrt{\pi}} \frac{\Gamma(5/6)}{\Gamma(1/3)} \frac{\overline{u^2}}{k_e} \frac{1}{\left[1 + (k_x/k_e)^2\right]^{5/6}} \tag{2}$$

and the upwash velocity component

$$\Theta_{vv}(k_x) = \frac{2}{27\sqrt{\pi}} \frac{\Gamma(5/6)}{\Gamma(7/3)} \frac{\overline{v^2}}{k_e} \frac{3 + 8(k_x/k_e)^2}{\left[1 + (k_x/k_e)^2\right]^{\frac{11}{6}}} \tag{3}$$

have been shown in the plots as a reference for the upstream undistorted conditions. In these expressions, $\Gamma(\cdot)$ is the Gamma function, k_x indicates the wavenumber in the streamwise direction, while $k_e = \frac{\pi}{L_{uu}^x} \frac{\Gamma(5/6)}{\Gamma(1/3)}$ is defined as the wavenumber scale of the largest turbulent structures.

The spectra of the streamwise component for the NACA 0012 and the NACA 0012-103 are reported in fig. 3. A good agreement is obtained with respect to von Kármán spectrum for the frequency spectra sampled in the most upstream positions, while an evident decrease of the fluctuations of this component occurs as the stagnation point is approached. This behavior is in agreement with the findings of the RDT of Hunt [10], who determined that, for large-scale turbulent structures, the blockage caused by the presence of the body causes the streamwise component to decrease.

The resulting momentum transfer causes the fluctuations of the upwash velocity component to increase in the vicinity of the stagnation point. This trend is clearly noticeable in fig. 4 in the low-frequency range, associated with large

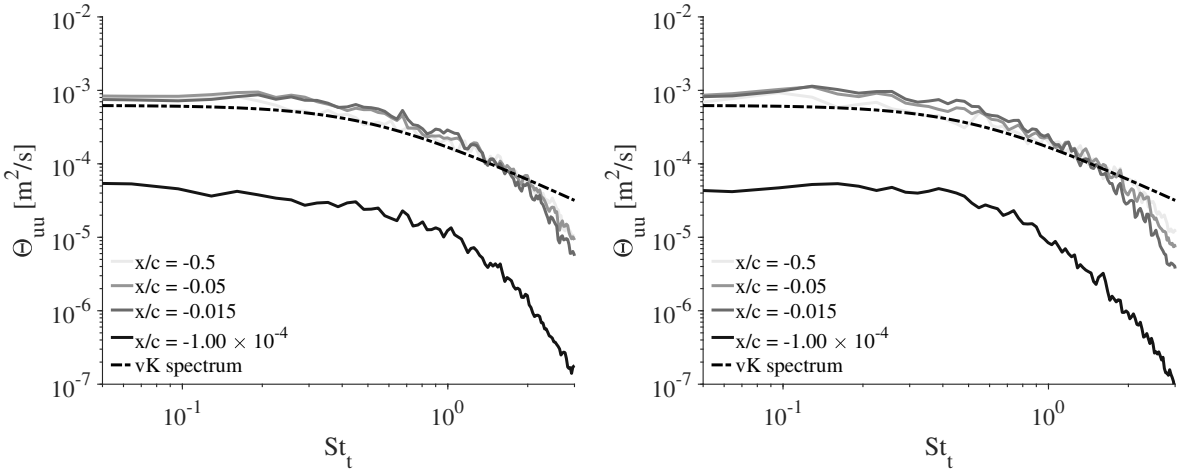

(a) NACA 0012 (b) NACA 0012-103

Fig. 3 Streamwise velocity component spectrum at different positions along the stagnation streamline. von Kármán spectrum has been reported as a reference.

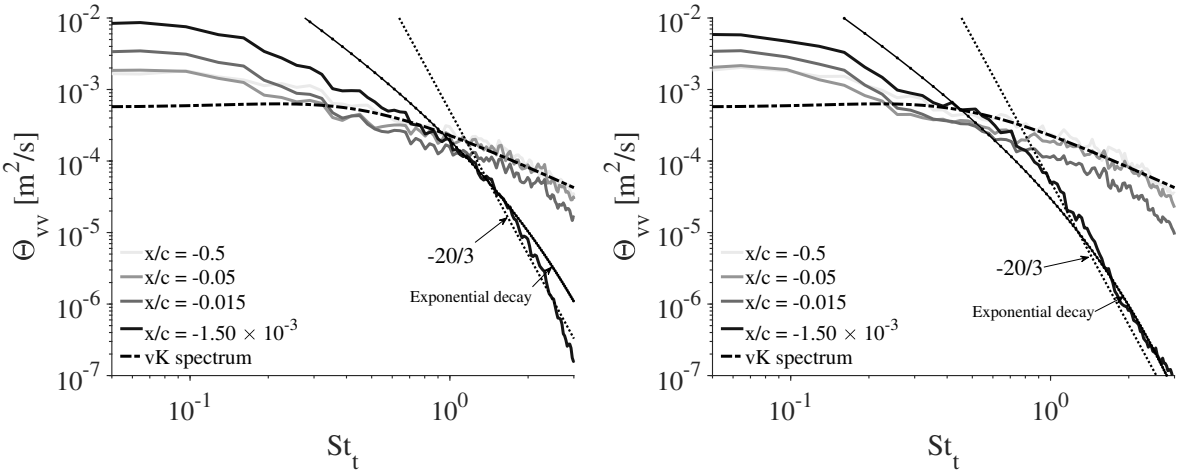

(a) NACA 0012 (b) NACA 0012-103

Fig. 4 Upwash velocity component spectrum at different positions along the stagnation streamline. von Kármán spectrum and the high-frequency decay slope have been reported as a reference.

turbulence scales, with respect to the spectra sampled more upstream. These are almost coincident with the reference von Kármán spectrum, with the exception of a small discrepancy at low frequencies.

Differently from the streamwise velocity component, the upwash velocity component spectra are characterized by a different behavior in the high-frequency range. Indeed, a progressive decrease can be observed for both airfoils with respect to upstream undistorted conditions. This is due to the distortion of the vorticity field, which affects the velocity fluctuations through the stretching or shortening of the vortex lines as they are convected towards the surface [10]. In particular, the upwash velocity component fluctuations have been proved to decrease, consistently with the present observations.

Interestingly, the high-frequency decay slope for frequency spectra sampled in the vicinity of the stagnation point features an exponential trend, as shown in fig. 4(a) for the NACA 0012 and in fig. 4(b) for the NACA 0012-103. The same results had been achieved analytically by Hunt [10] in the asymptotic analysis carried out in the simplifying assumption of very small turbulent scales with respect to the size of the body. In addition, it can be noticed that this

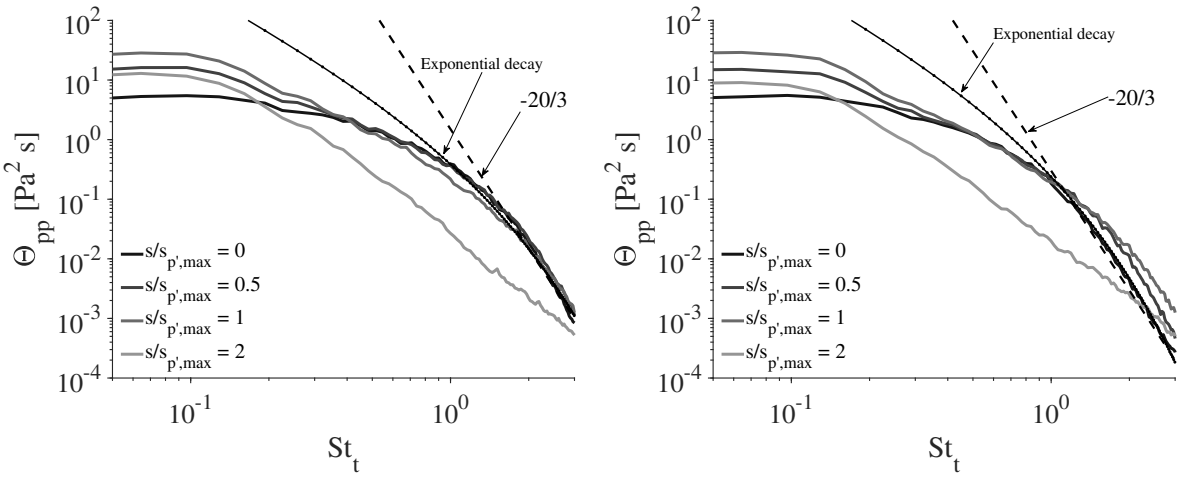

(a) NACA 0012 (b) NACA 0012-103

Fig. 5 Surface-pressure spectra at the airfoil leading edge. The distances along the airfoil surface have been set as multiples of the curvilinear abscissa $s_{p',\max}/c$ where the root-mean-square of the surface-pressure fluctuation is maximum.

exponential decay, for both airfoils, is very close to a $-20/3$ linear slope.

The analysis of the velocity field is combined with the investigation of the unsteady loading on the airfoil surface. In particular, surface-pressure spectra have been considered in the vicinity of the stagnation point to obtain information about the sound-production mechanisms. The sampling positions have been set as multiples of the curvilinear abscissa s, taken with respect to the stagnation point, where the fluctuations of the surface pressure peak. This position is equal to $s_{p',\max}/c = 0.016$ for the NACA 0012 and to $s_{p',\max}/c = 0.026$. Figure 5 reports these spectra for the NACA 0012 and the NACA 0012-103 in four different positions downstream of the stagnation point. In both cases, an exponential decay can be observed at high frequencies for the spectra sampled at the stagnation point. This behavior agrees with the study of Durbin and Hunt [28], who obtained the same finding in their analytical investigation. As for the velocity field, also for the surface-pressure spectra this exponential decay can be approximated by a linear trend with a slope equal to $-20/3$, which is consistent with the findings of the experimental campaign of Bowen et al. [9]. This slope decreases for the spectra considered at more downstream positions, which also feature an increase at low frequencies. This can probably be attributed to the effect of the large turbulent structures whose distortion has been shown to alter the velocity spectra similarly in this frequency range.

It can be concluded that the vorticity distortion occurring in the case of thick airfoil geometries, through the alteration of the velocity field in the stagnation region, significantly impacts the surface-pressure distribution at the leading edge. This is indeed induced by this same altered velocity field, indicating that noise generation is indeed affected by the distortion caused by the non-negligible thickness of the airfoil.

B. Effects of turbulence distortion on spanwise coherence length

The formulation of Amiet's model in the assumption of large span (eq. (1) introduces the spanwise coherence length of the upwash velocity component to account for the spanwise characteristics of the perturbation, for which an analytical expression (eq. (9)) was proposed. The accuracy of this equation has been assessed by comparing it with the spanwise coherence length calculated at the 4 sampling positions where the frequency spectra of the velocity components have been evaluated. The analysis is reported in fig. 6 for the NACA 0012 and the NACA 0012-103. The expression formulated by Amiet provides a good prediction of the spanwise coherence length at high frequencies, while an evident discrepancy is retrieved in the low-frequency range.

In addition, it must be noted that the spanwise coherence lengths calculated in the vicinity of the stagnation point feature an increase at low frequencies with respect to the ones calculated upstream. This alteration is due to the same mechanism observed for the frequency spectrum of the upwash velocity component, i.e. the transfer of momentum from the streamwise velocity component.

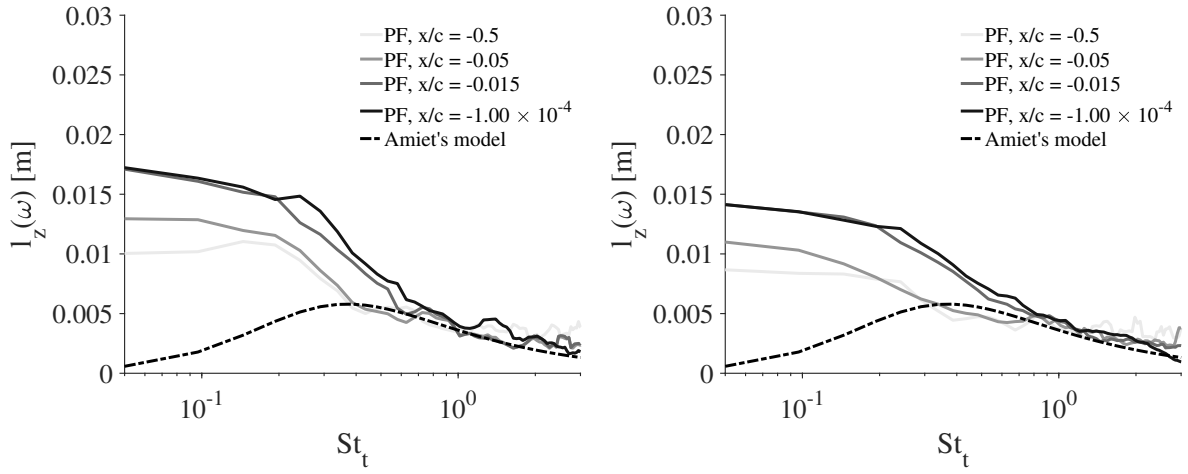

(a) NACA 0012 (b) NACA 0012-103

Fig. 6 Comparison between the spanwise coherence length calculated at different distances from the stagnation point along the stagnation streamline and the analytical model provided by Amiet.

These results reveal an insufficient knowledge as regards the description and the modeling of physical mechanisms affecting spanwise coherence length. Nevertheless, such advancements are crucial for developing enhancement methodologies for leading-edge noise prediction.

C. Impact of distortion mechanism on low-fidelity noise prediction

The impact of the alteration occurring in the stagnation region of the airfoil on the noise generation and modeling can be evaluated by using these altered turbulence conditions as inputs in Amiet's model. This low-fidelity method is usually implemented using as input canonical expressions as the one formulated by von Kármán or Liepmann to model undistorted flow conditions [15]. However, in order to directly assess the repercussions of the physical behaviors observed in the previous subsections, the upwash velocity spectrum and the spanwise coherence length *sampled* in the numerical flow field will be employed as input in the model. Amiet's model using as input the frequency spectrum and the spanwise coherence sampled at the most upstream position among the ones in table 2 is compared to the implementation using the quantities sampled at the closest position to the stagnation point. The results provided by the solid formulation of FWH analogy have been used as a reference.

Figure 7 shows this comparison for the NACA 0012 and the NACA 0012-103 in terms of sound pressure level (SPL) for a listener placed above the leading edge (azimuthal angle $\theta = 90°$) at $R = 1.2$ m. Amiet's model using as input the upstream flow quantities, as expected and consistently with the findings of the literature, provides a good agreement in the low-frequency range with respect to the noise prediction provided by FWH, while it does not match the decay at high frequencies. On the other hand, the implementation of the model featuring as input the altered frequency spectrum and spanwise coherence length provides an excellent prediction of this decay, while overestimating the noise levels of a constant offset of 6 dB on the whole frequency range. The same conclusions can be drawn from the analysis of the sound power level (PWL) for the two airfoils reported in fig. 8.

A different formulation of Amiet's model has been implemented to investigate the effects of turbulence distortion on noise generation. Equation (7), relating the cross-spectral density of the surface-pressure fluctuations to the far-field noise, has been applied using as input the unsteady loading distribution on the airfoil surfaces. This implies that no transfer function is involved to retrieve the pressure jump on the airfoil surface from the turbulence characteristics. As for the previous implementation, the analysis has been conducted in terms of SPL for a listener above the leading edge and PWL, shown respectively in fig. 9 and fig. 10. An excellent agreement is obtained for the two airfoils with respect to the results of the FWH analogy, both in terms of noise levels and high-frequency decay slope. The discrepancy at high frequencies is caused by the numerical solution of equation 7. Indeed, the high computational cost of the implementation prevents the spatial resolution of the surface-pressure sampling from being further increased, causing destructive interference effects to be underestimated.

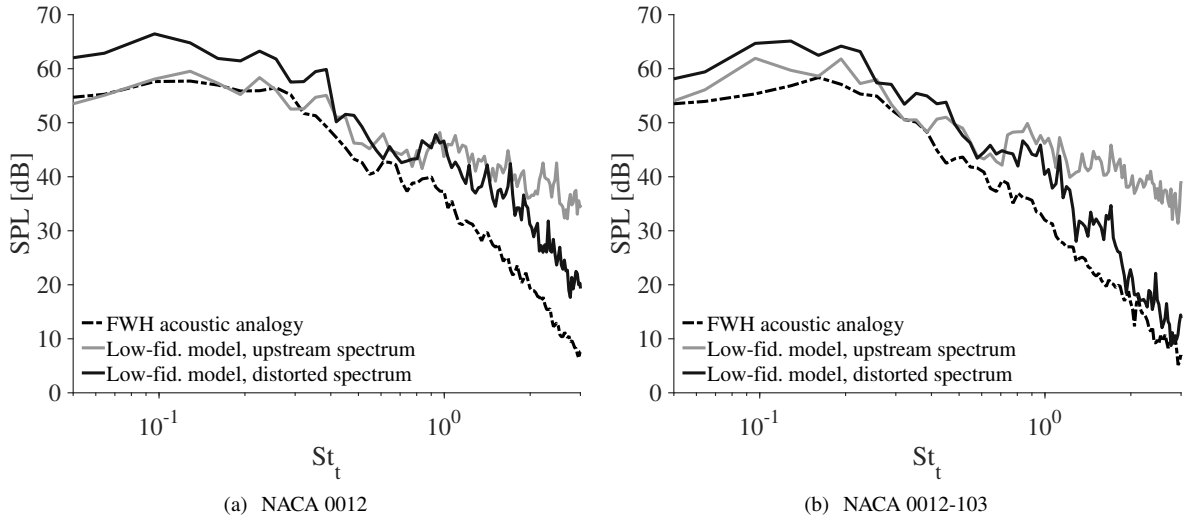

(a) NACA 0012 (b) NACA 0012-103

Fig. 7 Comparison in terms of sound pressure level between Amiet's model implementation using turbulence characteristics sampled in the upstream undistorted region of the flow field and in the altered region close to the stagnation point. The listener is placed above the leading edge ($R = 1.2$ m, $\theta = 90°$) and the results provided by the FWH acoustic analogy are included as a reference.

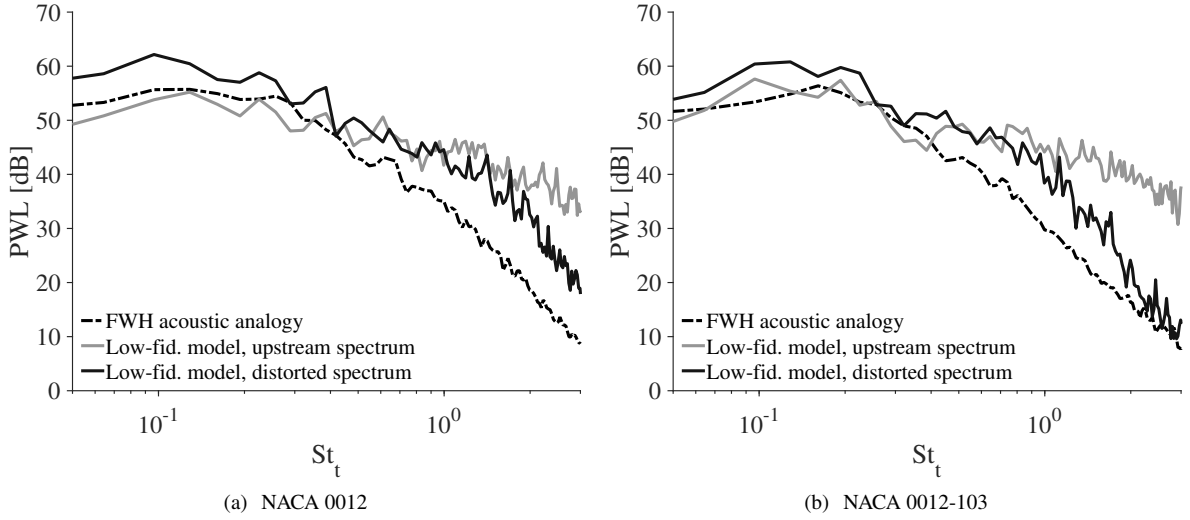

(a) NACA 0012 (b) NACA 0012-103

Fig. 8 Comparison in terms of sound power level between Amiet's model implementation using turbulence characteristics sampled in the upstream undistorted region of the flow field and in the altered region close to the stagnation point. The results provided by the FWH acoustic analogy are included as a reference.

These results demonstrate that the inclusion of turbulence-distortion effects into low-fidelity models represents a more accurate modeling of noise-generation mechanisms and can hence lead to improved noise predictions. This can be done by considering turbulence characteristics in the immediate vicinity of the stagnation point, in order to account for the physical mechanisms characterizing the unsteady surface pressure distribution at the leading edge. Nevertheless, this modification leads to overestimating the noise levels of a constant offset over the whole frequency range. Insight about this discrepancy is provided by the comparison with the formulation of Amiet's model retrieving far-field acoustic pressure directly from the unsteady loading distribution, whose noise prediction coincides with the one yielded by FWH analogy. Indeed, the fact that this implementation does not rely on the employment of the aeroacoustic transfer function suggests that the modeling of the airfoil aerodynamic and acoustic response requires further advancements to account

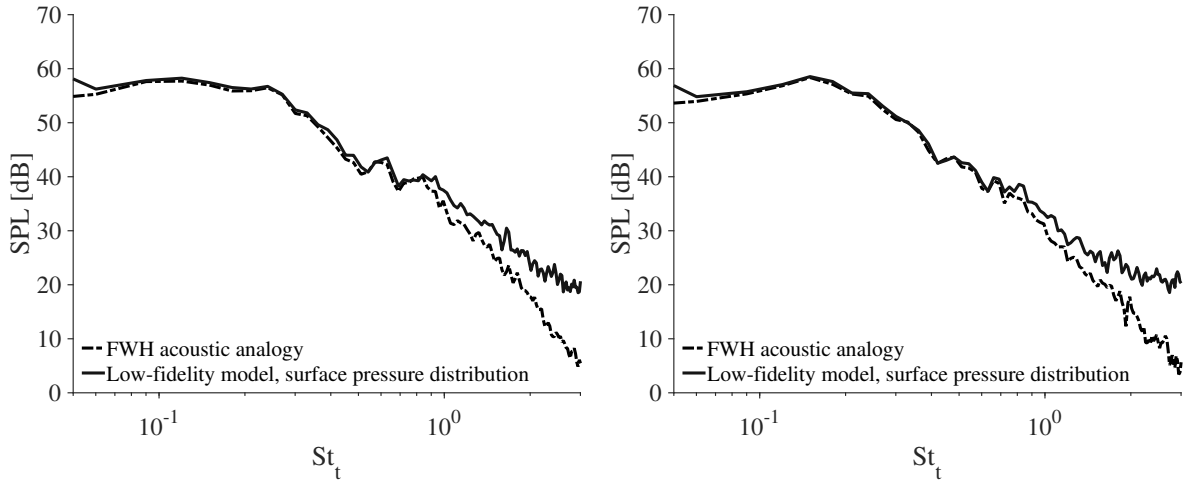

(a) NACA 0012 (b) NACA 0012-103

Fig. 9 Sound pressure level provided by Amiet's formulation using the cross-spectral density of surface-pressure fluctuations as input. The listener is placed above the leading edge ($R = 1.2\,\mathrm{m}, \theta = 90°$) and the results provided by the FWH acoustic analogy are included as a reference.

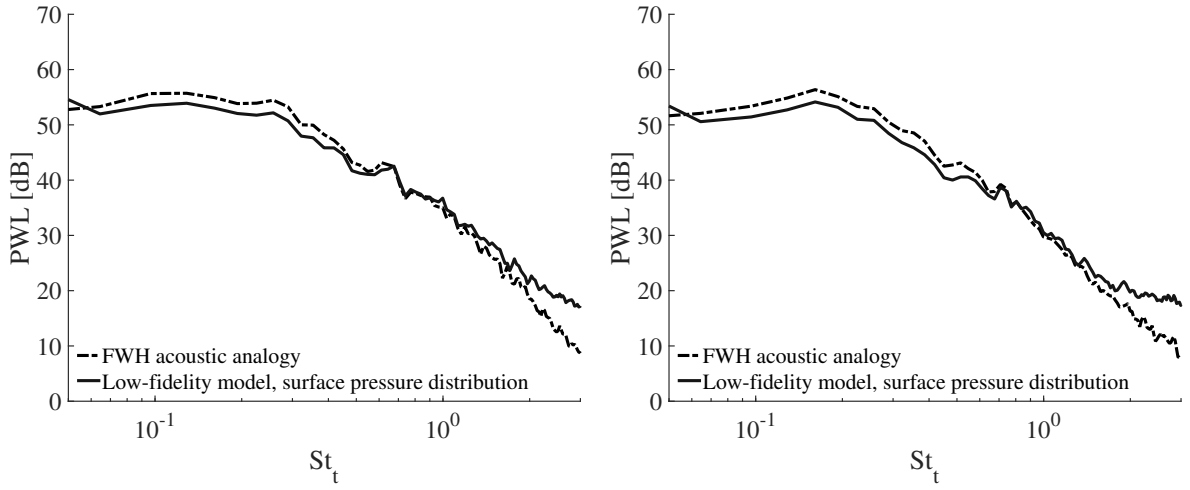

(a) NACA 0012 (b) NACA 0012-103

Fig. 10 Sound power level provided by Amiet's formulation using the cross-spectral density of surface-pressure fluctuations as input. The results provided by the FWH acoustic analogy are included as a reference.

for the effects of turbulence distortion due to realistic airfoil geometry.

IV. Conclusions

A physical evaluation of the alterations of the flow field due to the distortion of turbulent structures interacting with the leading edge of thick airfoils has been conducted in this study. The purpose was the assessment of possible enhancement methodologies for leading-edge noise prediction by means of low-fidelity models. The analysis has been carried out in the framework of Amiet's theory, widely investigated in the academic and industrial sectors, which models the turbulence conditions in terms of frequency spectrum and spanwise coherence length of the upwash velocity component.

For this purpose, the interaction of grid-generated turbulence with a NACA 0012 and a NACA 0012-103, featuring the

same thickness but different leading-edge shape, have been investigated numerically using the LBM solver PowerFLOW. The numerical set-up reproduces the one employed by Chaitanya et al. [8], who conducted a wide experimental campaign focused on leading-edge noise analysis.

The distortion of the turbulent eddies has been shown to alter the frequency spectrum of the streamwise and the upwash velocity component in the immediate vicinity of the stagnation point. In particular, the frequency spectra of the upwash velocity component in the vicinity of the stagnation point have been shown to exhibit an exponential decay slope in the high-frequency range. The same behavior characterizes the high-frequency decay of surface-pressure spectra sampled close to the leading edge. This result leads to a twofold conclusion: it not only proves that the unsteady loading at the leading edge is induced by the altered velocity field in the vicinity of the leading edge, demonstrating that turbulence distortion does affect surface-pressure distribution, but also suggests that noise generation is indeed impacted by these physical mechanisms. The conclusion is that an accurate modeling of the alteration caused by the distortion of the turbulent eddies must be included in low-fidelity noise-prediction methods.

The analysis of the spanwise coherence length of the upwash velocity component leads to the same conclusions. Indeed, the comparison between the numerical calculations and the equation proposed by Amiet to model this quantity reveals a significant discrepancy, indicating a deficiency in the current analytical prediction accuracy. In addition, spanwise coherence lengths sampled in the stagnation region are characterized by the same increase at low frequencies observed for the frequency spectra of the upwash velocity component, as expected.

The effects of these alterations on the velocity and surface-pressure field on low-fidelity noise prediction have been investigated by applying Amiet's model using as input the velocity spectra and the coherence length directly calculated from the numerical data sampled in the domain. Indeed, with respect to the implementation of Amiet's model sampling flow characteristics in the upstream undistorted region of the flow field, the one considering turbulence conditions close to the stagnation point retrieves an improved prediction of the decay slope at low and high frequencies. However, this application of Amiet's model provides a constant overestimation of the noise levels of 6 dB with respect to the results obtained with FWH analogy, probably due to an insufficient characterization of the distortion effects on the aerodynamic and acoustic response of the airfoil, modeled by means of the aeroacoustic transfer function.

In conclusion, while the definition of this physical framework lays the ground for potential enhancement methodologies of low-fidelity noise-prediction methods, it also highlights the need for further advancements to improve the modeling of flow-field alterations and describe their impact on the aeroacoustic transfer function.

A. Grid-independence study

The analysis of the numerical effects due to the discretization of the domain has been carried out only for the NACA-0012 case. Three different resolution levels have been taken into account: a coarse, a medium, and a fine one, with these two obtained by refining the first one of a factor 1.5 and 2, respectively. This results in a resolution, assessed in terms of size of the smallest voxel with respect to the leading-edge radius, equal to 6.62, 9.93 and 13.25 for the three cases. The total amount of voxels is 91×10^6 for the coarse configuration, 287×10^6 for the medium one, and 660×10^6 for the fine. The independence of the results from the grid discretization has been investigated in terms of sound power level (PWL) and time-averaged lift and drag, integrated on the whole airfoil surface.

The comparison between the PWL obtained experimentally by Chaitanya et al. [8] and the ones calculated with the FWH analogy in the three resolution configurations is shown in fig. 11 with respect to the Strouhal number St_t (where t is the airfoil thickness). Leading-edge noise is the dominant noise source in the frequency range between $St_t = 0.15$ and $St_t = 1.5$, highlighted in the figure [8]. At lower frequencies ($St_t < 0.15$), background noise dominates, while for $St_t < 1.5$ airfoil self noise is prevailing. The similarity of the three curves, which are almost coincident in the frequency range of interest for the analysis of leading-edge noise, demonstrates the numerical convergence of the simulations.

Figure 12 shows the trend of the time-averaged lift coefficient C_L and drag coefficient C_D as a function of the total number of voxels for the three resolution configurations. While the drag coefficient tends to a constant value, confirming that the simulation has reached convergence, the trend of C_L is affected by slight oscillations. However, by taking into account the lift curve of a NACA 0012 at the $Re_c = 6.2 \times 10^5$, it results that this lift oscillation corresponds to a variation of the angle of attack of $\simeq 0.25°$, negligible in the case of an airfoil interacting with a strongly turbulent flow.

B. Amiet's theory

Low-fidelity method formulated by Amiet [1] to predict far-field noise radiated by an airfoil in a turbulent flow is briefly detailed here. It must be underlined that with respect to the original notation, the one used here has been modified

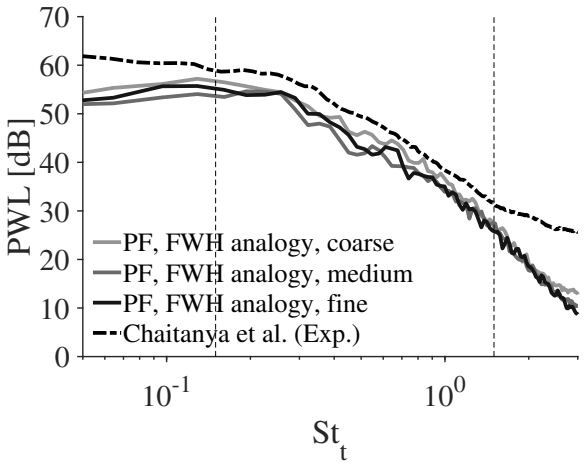

Fig. 11 Sound power level at three different grid resolutions of the NACA-0012 case for the numerical convergence analysis.

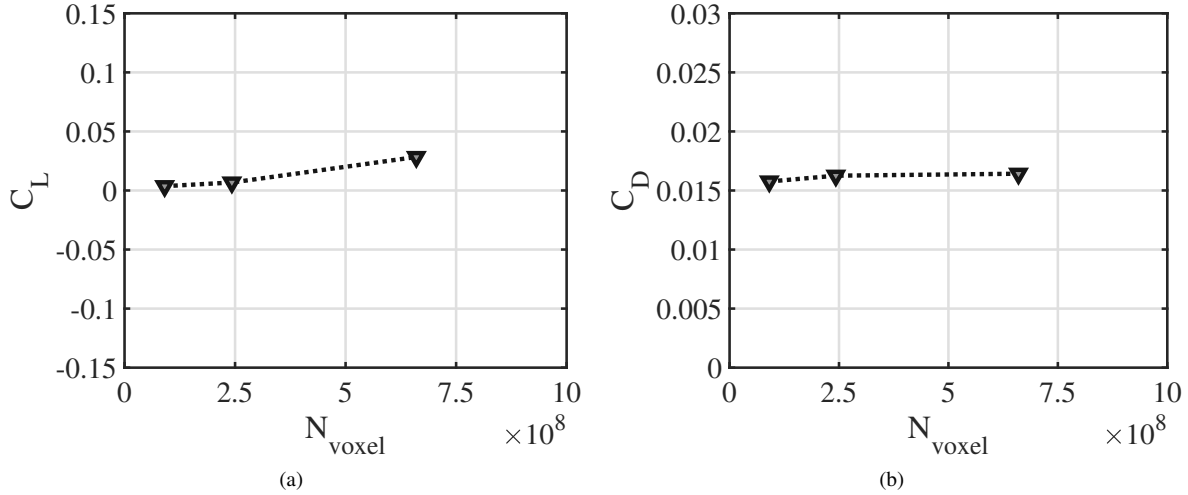

Fig. 12 Trends of the time-averaged (a) lift coefficient C_L and (b) drag coefficient C_D, integrated along the airfoil surface, at the three different resolution configurations for the NACA-0012 case.

for consistency with the reference system of the numerical domain. The x-axis will hence indicate the streamwise direction, the y-axis the upwash direction and the z-axis the spanwise one, while the velocity components will be indicated with u, v and w, respectively.

The model was developed starting from two underlying assumptions: the turbulence is assumed to be frozen and the airfoil is simplified into a flat plate. This allows, for the linearized theory, the interaction to be modeled in terms of the wavenumber k_x and k_z and to neglect any contribution associated with k_y. A monochromatic sinusoidal gust with amplitude v_0 and transverse wavenumbers k_x and k_z expressed as

$$v_g = v_0 \mathrm{e}^{\mathrm{i}[k_x(U_\infty t - x) - k_z z]} \tag{4}$$

is hence considered to induce the unsteady loading through

$$\Delta p\,(x, z, t) = \pi \rho_\infty U_\infty \mathrm{c} v_0 g(x, k_x, k_z) \mathrm{e}^{\mathrm{i}(k_z z - k_x U_\infty t)}, \tag{5}$$

with $g\left(x, k_x, k_y\right)$ being the transfer function relating the pressure jump $\Delta p\,(x, y, t)$ on the aerodynamic surface to the incoming perturbation. In this framework, any effect due to realistic geometrical features of the airfoil on the

sound radiation is considered negligible. Under these hypotheses, the final expression to predict far-field noise power spectral density $S_{pp}(\omega)$ at listener location $\boldsymbol{x} = (x, y, z)$ generated by an airfoil of chord c and span L interacting with a turbulent flow convected at free-stream velocity U_∞ will be

$$S_{pp}(\boldsymbol{x}, \omega) = \left(\frac{\omega y \rho_\infty \mathrm{c}}{2\mathrm{c}_\infty \sigma^2}\right)^2 \pi U_\infty \frac{\mathrm{L}}{2} \int_{-\infty}^{+\infty} \frac{\sin^2\left[\frac{\mathrm{L}}{2}\left(k_z + \frac{\omega z}{\mathrm{c}_\infty \sigma}\right)\right]}{\left(k_z + \frac{\omega z}{\mathrm{c}_\infty \sigma}\right)^2 \pi \frac{\mathrm{L}}{2}} \left|\mathcal{L}(\boldsymbol{x}, K_x, k_z)\right|^2 \Phi_{vv}(K_x, k_z)\, \mathrm{d}k_z, \tag{6}$$

where $\sigma = \sqrt{(x - x_0)^2 + \beta^2\left[(y - y_0)^2 + (z - z_0)^2\right]}$ takes into account the convection effects and $\beta = \sqrt{1 - M^2}$ being the compressibility factor. $K_x = \frac{-\omega}{U_\infty}$ for the assumption of frozen turbulence. This equation is retrieved from the one relating far-field acoustic pressure to the cross-spectral density of the surface pressure S_{QQ}

$$S_{pp}(\boldsymbol{x}, \omega) = \left(\frac{\omega z}{4\pi c_0 \sigma^2}\right)^2 \iiiint S_{QQ}(x_1, x_2, \eta, \omega) \times \mathrm{e}^{\frac{\mathrm{i}\omega}{c_0}\left[\beta^{-2}(x_1 - x_2)\left(M - \frac{x}{\sigma}\right) + \frac{y\eta}{\sigma}\right]} \mathrm{d}x_1 \mathrm{d}x_2 \mathrm{d}y_1 \mathrm{d}y_2. \tag{7}$$

Φ_{vv} is in turn related to S_{QQ} by converting into statistical quantities the deterministic ones in eq. (5).

Equation (6) can be simplified, in the assumption of large span, in eq. (1), which features the frequency spectrum of the upwash-velocity component $\Theta_{vv}(\omega)$ and the spanwise coherence length $l_z(\omega)$ to describe the incoming turbulence characteristics in place of the wavenumber spectrum $\Phi_{vv}(\omega)$. This is obtained through the following expression

$$l_z(\omega) = \frac{\pi}{U_\infty} \frac{\Phi_{vv}(K_x, 0)}{\Theta_{vv}(\omega)}. \tag{8}$$

By modeling $\Phi_{vv}(\omega)$ and $\Theta_{vv}(\omega)$ by means of the von Kármán expressions, respectively equal to

$$\Phi_{vv}(k_x, k_y) = \frac{4}{9\pi} \frac{\overline{u^2}}{k_e^2} \frac{(k_x/k_e)^2 + (k_y/k_e)^2}{\left[1 + (k_x/k_e)^2 + (k_y/k_e)^2\right]^{\frac{7}{3}}},$$

for the two-wavenumber spectrum and to eq. (3) for the frequency spectrum of the upwash velocity component, the following analytical expression is finally proposed by Amiet to model the spanwise coherence length

$$l_z(\omega) = \frac{8L}{3}\left[\frac{\Gamma(1/3)}{\Gamma(5/6)}\right]^2 \frac{(K_x/k_e)^2}{\left(3 + 8(K_x/k_e)^2\right)\sqrt{1 + (K_x/k_e)^2}}. \tag{9}$$

$\mathcal{L}$ indicates the aeroacoustic transfer function, which models the aerodynamic and acoustic response of the airfoil to the incoming perturbation. This is obtained through

$$\mathcal{L}(x, K_x, k_y) = \int_{-L/2}^{L/2} g(x_0, K_x, k_y)\, \mathrm{e}^{-\mathrm{i}\omega x_0 (M - x/\sigma)/c_\infty \beta^2} \mathrm{d}x_0. \tag{10}$$

References

[1] Amiet, R. K., "Acoustic Radiation from an Airfoil in a Turbulent Stream," *Journal of Sound and Vibration*, Vol. 41, No. 4, 1975, pp. 407–420. https://doi.org/10.1016/S0022-460X(75)80105-2.

[2] Paterson, R., and Amiet, R., "Acoustic Radiation and Surface Pressure Characteristics of an Airfoil Due to Incident Turbulence," *3rd Aeroacoustics Conference*, Aeroacoustics Conferences, American Institute of Aeronautics and Astronautics, 1976. https://doi.org/10.2514/6.1976-571.

[3] Olsen, W., and Wagner, J., "Effect of Thickness on Airfoil Surface Noise," *AIAA Journal*, Vol. 20, No. 3, 1982, pp. 437–439. https://doi.org/10.2514/3.7922.

[4] Moriarty, P., Guidati, G., and Migliore, P., "Recent Improvement of a Semi-Empirical Aeroacoustic Prediction Code for Wind Turbines," *10th AIAA/CEAS Aeroacoustics Conference*, American Institute of Aeronautics and Astronautics, Manchester, GREAT BRITAIN, 2004. https://doi.org/10.2514/6.2004-3041.

[5] Goldstein, M. E., and Atassi, H., "A Complete Second-Order Theory for the Unsteady Flow about an Airfoil Due to a Periodic Gust," *Journal of Fluid Mechanics*, Vol. 74, No. 4, 1976, pp. 741–765. https://doi.org/10.1017/S0022112076002036.

[6] Oerlemans, S., "Wind Tunnel Aeroacoustic Tests of Six Airfoils for Use on Small Wind Turbines; Period of Performance: August 23, 2002 through March 31, 2004," Tech. Rep. NREL/SR-500-35339, 15007773, Aug. 2004. https://doi.org/10.2172/15007773.

[7] Hall, A., Atassi, O., Gilson, J., Reba, R., and Shannon, D., "Effect of Leading-Edge Thickness on High-Speed Airfoil-Turbulence Interaction Noise," *17th AIAA/CEAS Aeroacoustics Conference (32nd AIAA Aeroacoustics Conference)*, Aeroacoustics Conferences, American Institute of Aeronautics and Astronautics, 2011. https://doi.org/10.2514/6.2011-2861.

[8] Chaitanya, P., Gill, J. R., Narayanan, S., Joseph, P., Vanderwel, C., Zhang, X., and Ganapathisubramani, B., "Aerofoil Geometry Effects on Turbulence Interaction Noise," *21st AIAA/CEAS Aeroacoustics Conference*, AIAA AVIATION Forum, American Institute of Aeronautics and Astronautics, 2015. https://doi.org/10.2514/6.2015-2830.

[9] Bowen, L., Celik, A., and Azarpeyvand, M., "A Thorough Experimental Investigation on Airfoil Turbulence Interaction Noise," *Physics of Fluids*, Vol. 35, No. 3, 2023, p. 035123. https://doi.org/10.1063/5.0142704.

[10] Hunt, J. C. R., "A Theory of Turbulent Flow Round Two-Dimensional Bluff Bodies," *J. Fluid Mech.*, Vol. 61, No. 4, 1973, pp. 625–706. https://doi.org/10.1017/S0022112073000893.

[11] Mish, P., and Devenport, W., "An Experimental Investigation of Unsteady Surface Pressure on an Airfoil in Turbulence—Part 1: Effects of Mean Loading," *Journal of Sound and Vibration*, Vol. 296, No. 3, 2006, pp. 417–446. https://doi.org/10.1016/j.jsv.2005.08.008.

[12] Mish, P., and Devenport, W., "An Experimental Investigation of Unsteady Surface Pressure on an Airfoil in Turbulence—Part 2: Sources and Prediction of Mean Loading Effects," *Journal of Sound and Vibration*, Vol. 296, No. 3, 2006, pp. 447–460. https://doi.org/10.1016/j.jsv.2005.08.009.

[13] Moreau, S., and Roger, M., "Effect of Angle of Attack and Airfoil Shape on Turbulence-Interaction Noise," *11th AIAA/CEAS Aeroacoustics Conference*, American Institute of Aeronautics and Astronautics, Monterey, California, 2005. https://doi.org/10.2514/6.2005-2973.

[14] Christophe, J., "Application of Hybrid Methods to High Frequency Aeroacoustics," Ph.D. thesis, 2011.

[15] De Santana, D., Christophe, J., Schram, C., and Desmet, W., "A Rapid Distortion Theory Modified Turbulence Spectra for Semi-Analytical Airfoil Noise Prediction," *Journal of Sound and Vibration*, Vol. 383, 2016, pp. 349–363. https://doi.org/10.1016/j.jsv.2016.07.026.

[16] dos Santos, F. L., Botero-Bolívar, L., Venner, C., and De Santana, L., "Modeling the Turbulence Spectrum Dissipation Range for Leading-Edge Noise Prediction," *AIAA Journal*, 2022, pp. 1–12. https://doi.org/10.2514/1.J061106.

[17] dos Santos, F. L., Botero Bolivar, L., Venner, C., and De Santana, L., "Inflow Turbulence Distortion for Airfoil Leading-Edge Noise Prediction for Large Turbulence Length Scales for Zero-Mean Loading," *The Journal of the Acoustical Society of America*, Vol. 153, 2023, pp. 1811–1822. https://doi.org/10.1121/10.0017458.

[18] Piccolo, A., Zamponi, R., Avallone, F., and Ragni, D., "Turbulence-Distortion Analysis for Leading-Edge Noise-Prediction Enhancement," *AIAA AVIATION 2023 Forum*, AIAA AVIATION Forum, American Institute of Aeronautics and Astronautics, 2023. https://doi.org/10.2514/6.2023-3628.

[19] Chen, H., Chen, S., and Matthaeus, W. H., "Recovery of the Navier-Stokes Equations Using a Lattice-Gas Boltzmann Method," *Phys. Rev. A*, Vol. 45, No. 8, 1992, pp. R5339–R5342. https://doi.org/10.1103/PhysRevA.45.R5339.

[20] Succi, S., *The Lattice Boltzmann Equation: For Fluid Dynamics and Beyond*, Numerical Mathematics and Scientific Computation, Oxford University Press, Oxford, New York, 2001.

[21] Bhatnagar, P. L., Gross, E. P., and Krook, M., "A Model for Collision Processes in Gases. I. Small Amplitude Processes in Charged and Neutral One-Component Systems," *Phys. Rev.*, Vol. 94, No. 3, 1954, pp. 511–525. https://doi.org/10.1103/PhysRev.94.511.

[22] Yakhot, V., and Orszag, S., "Renormalization Group Analysis of Turbulence. I. Basic Theory," *J Sci Comput*, Vol. 1, No. 1, 1986, pp. 3–51. https://doi.org/10.1007/BF01061452.

[23] Yakhot, V., Orszag, S. A., Thangam, S., Gatski, T. B., and Speziale, C. G., "Development of Turbulence Models for Shear Flows by a Double Expansion Technique," *Physics of Fluids A: Fluid Dynamics*, Vol. 4, No. 7, 1992, pp. 1510–1520. https://doi.org/10.1063/1.858424.

[24] Farassat, F., and Succi, G. P., "A Review of Propeller Discrete Frequency Noise Prediction Technology with Emphasis on Two Current Methods for Time Domain Calculations," *Journal of Sound and Vibration*, Vol. 71, No. 3, 1980, pp. 399–419. https://doi.org/10.1016/0022-460X(80)90422-8.

[25] Casalino, D., "An Advanced Time Approach for Acoustic Analogy Predictions," *Journal of Sound and Vibration*, Vol. 261, No. 4, 2003, pp. 583–612. https://doi.org/10.1016/S0022-460X(02)00986-0.

[26] Curle, N., and Lighthill, M. J., "The Influence of Solid Boundaries upon Aerodynamic Sound," *Proceedings of the Royal Society of London. Series A. Mathematical and Physical Sciences*, Vol. 231, No. 1187, 1955, pp. 505–514. https://doi.org/10.1098/rspa.1955.0191.

[27] Roach, P. E., "The Generation of Nearly Isotropic Turbulence by Means of Grids," *International Journal of Heat and Fluid Flow*, Vol. 8, No. 2, 1987, pp. 82–92. https://doi.org/10.1016/0142-727X(87)90001-4.

[28] Durbin, P. A., and Hunt, J. C. R., "On Surface Pressure Fluctuations beneath Turbulent Flow Round Bluff Bodies," *Journal of Fluid Mechanics*, Vol. 100, No. 1, 1980, pp. 161–184. https://doi.org/10.1017/S0022112080001061.